JACS
JOURNAL OF THE AMERICAN CHEMICAL SOCIETY

pubs.acs.org/JACS

Article

Disparity of Cytochrome Utilization in Anodic and Cathodic Extracellular Electron Transfer Pathways of *Geobacter sulfurreducens* Biofilms

Nina Heidary,[§] Nikolay Kornienko,[§] Shafeer Kalathil, Xin Fang, Khoa H. Ly, Heather F. Greer, and Erwin Reisner*

Cite This: *J. Am. Chem. Soc.* 2020, 142, 5194−5203

Read Online

ACCESS | Metrics & More | Article Recommendations | Supporting Information

ABSTRACT: Extracellular electron transfer (EET) in microorganisms is prevalent in nature and has been utilized in functional bioelectrochemical systems. EET of *Geobacter sulfurreducens* has been extensively studied and has been revealed to be facilitated through *c*-type cytochromes, which mediate charge between the electrode and *G. sulfurreducens* in anodic mode. However, the EET pathway of cathodic conversion of fumarate to succinate is still under debate. Here, we apply a variety of analytical methods, including electrochemistry, UV−vis absorption and resonance Raman spectroscopy, quartz crystal microbalance with dissipation, and electron microscopy, to understand the involvement of cytochromes and other possible electron-mediating species in the switching between anodic and cathodic reaction modes. By switching the applied bias for a *G. sulfurreducens* biofilm coupled to investigating the quantity and function of cytochromes, as well as the emergence of Fe-containing particles on the cell membrane, we provide evidence of a diminished role of cytochromes in cathodic EET. This work sheds light on the mechanisms of *G. sulfurreducens* biofilm growth and suggests the possible existence of a nonheme, iron-involving EET process in cathodic mode.

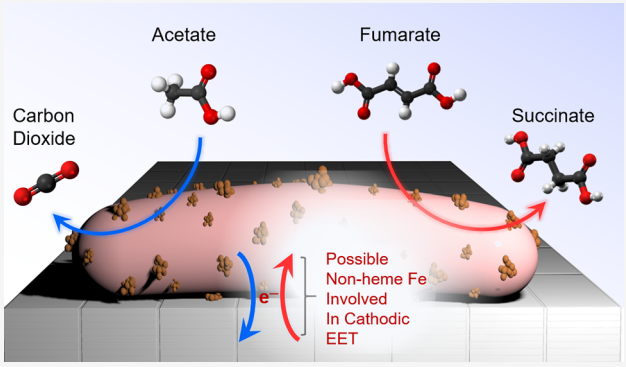

INTRODUCTION

Electroactive bacteria are ubiquitous in environments ranging from the soil and wastewater to deep-sea hydrothermal vents and the human digestive system.[1−3] At an applied level, electroactive microbes show promise in microbial fuel cells (MFCs),[4] microbial electrosynthesis of value-added chemicals,[5,6] and as components of semiartificial photosynthetic systems.[7−9] Despite knowledge of their existence for over a century, precise mechanisms of charge transfer between the electrode and bacteria are still not fully elucidated.[10,11]

Geobacter sulfurreducens is a prototype electrogenic bacterium whose biofilms exhibit the highest current densities on electrodes to date with uses in MFCs.[12,13] Its growth and electrogenic behavior have been studied on a multitude of electrode surfaces at both a macroscopic and a single-cell level.[14,15] Oxidation of acetate to CO_2 is the model oxidation reaction investigated (anodic mode) (Figure 1a). Studies have postulated that its extracellular electron transfer (EET) proceeds through a pilus- and/or cytochrome-mediated pathway.[1,16−20] Recent works have implicated the involvement of riboflavin as well.[21,22] Research efforts have also shown that, under certain conditions, *G. sulfurreducens* can produce reductive currents at a negatively biased electrode stemming from reactions such as the reduction of fumarate to succinate (cathodic mode).[23,24] The precise mechanisms underlying cathodic mode EET are even more ambiguous than those governing anodic mode EET.[25,26] Several studies have proposed cytochromes, hydrogenases, and solubilized redox mediators as being potential channels for electron transfer in this configuration, though conclusive answers are not universally agreed upon.[27]

In this work, we carried out a multifaced study on the growth and electrogenesis of *G. sulfurreducens* in systematically switching between anodic and cathodic modes on inverse-opal indium tin oxide (IO−ITO) electrodes (Figure 1b). In addition to the conventional electrochemical experiments, we performed complementary studies using in situ resonance Raman spectroscopy, UV−vis absorption spectroscopy, quartz-crystal microbalance with dissipation (QCM-D) measurements, and ex situ scanning and transmission electron

Received: December 4, 2019
Published: February 17, 2020

https://dx.doi.org/10.1021/jacs.9b13077
J. Am. Chem. Soc. 2020, 142, 5194−5203

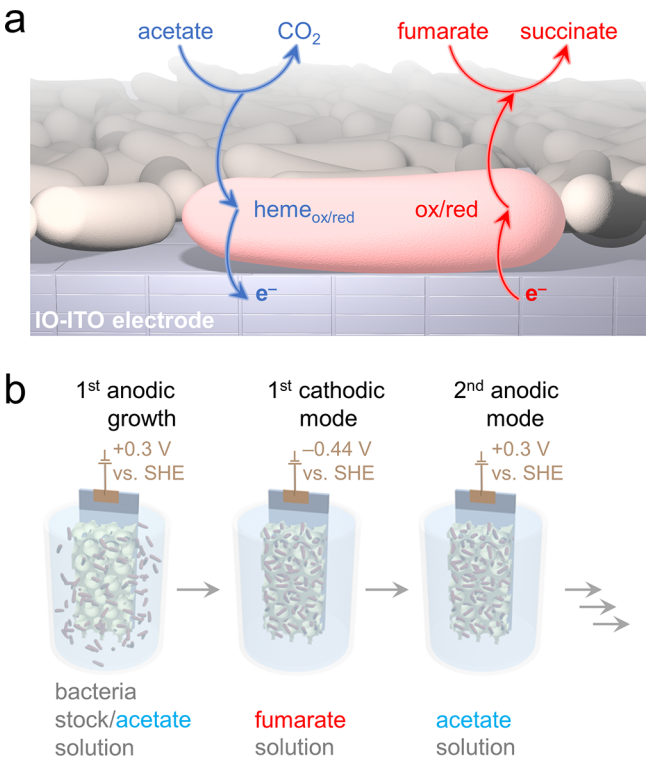

Figure 1. (a) Schematic representation of EET of *G. sulfurreducens* biofilm under anodic (acetate to CO_2) and cathodic (fumarate to succinate) conditions. (b) The biofilm was grown on the IO−ITO electrode under anodic conditions and sequentially switched between the two modes by switching the buffer medium and electrode polarization.

microscopy (SEM and TEM) to piece together clues behind the mechanisms of their anodic and cathodic electron transfer. Using this comprehensive set of measurements, we found that the anodic mode function is mainly linked to the biofilm's cytochrome expression, but the cathodic mode likely operates partially through an alternate channel. We propose that an Fe-containing soluble species that can either come from Fe ions in the medium or alternatively be scavenged from cytochromes is contributing to cathodic mode charge transfer under our set of reaction conditions. The presented findings add insight into *G. sulfurreducens*' function in its natural environments. At an applied level, they may also aid emerging biotechnologies. Finally, the results press for a closer look at the multitude of EET pathways present in biological systems.

RESULTS AND DISCUSSION

G. sulfurreducens biofilms were grown on IO−ITO electrodes, which were prepared through a hard-template method from polystyrene microspheres and ∼20 nm ITO nanoparticles (see Experimental Details).[28−30] IO−ITO with a macropore size of ∼10 μm was chosen because of its high degree of meso- and macroporosity that both facilitates mass transfer from the solution and features a high degree of surface area in its electrically conductive macropores.[30,31] This allows for the electrodes to accommodate a high geometric density of biofilm growth by facilitating the effective penetration of *G. sulfurreducens* cells which are approximately 0.2 μm in diameter and 2 μm in length.[30−32] The structure also enables biofilm growth in such a manner that most cells are directly wired to the electrode. The secondary benefit of using an ITO substrate is that it is optically transparent, allowing for in situ spectroscopic experiments to be carried out.[11,19,33] To grow biofilms, IO−ITO electrodes were immersed in a *G. sulfurreducens* medium (featuring acetate to be oxidized by the bacteria) in oxygen-free conditions and poised at ∼0.3 V vs SHE for 4 days.[30] SEM images acquired after a typical initial growth in anodic mode show *G. sulfurreducens* cells attached to the IO−ITO surface (Figure 2a and 2b).

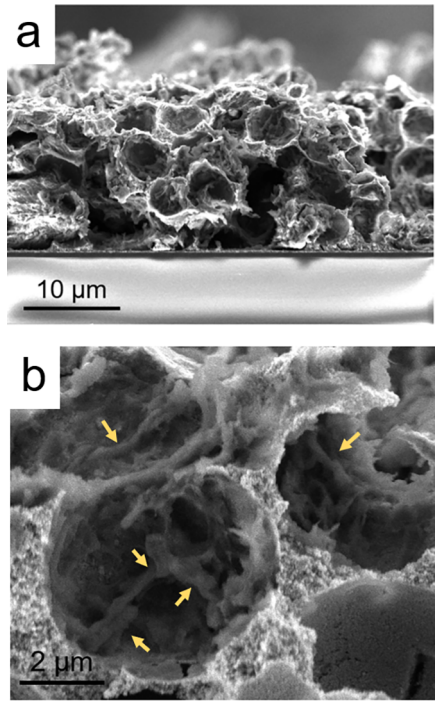

Figure 2. (a) SEM of cross section from *G. sulfurreducens* grown on IO−ITO at low and (b) high magnification. Yellow arrows point to *G. sulfurreducens* cells.

We subsequently explored the use of this IO−ITO electrode modified with *G. sulfurreducens* for growth and switching between anodic and cathodic modes (Figure 3). The first anodic growth resulting in biofilm formation onto the electrode featured a commonly observed lag phase followed by an exponential growth period and finally a current plateau at ∼2 mA cm^{-2}. The lag phase has previously been postulated as a period of cell attachment to the electrode surface and extracellular matrix formation prior to reproduction resulting in the exponential phase.[30,34] The current plateau is known to result from a mature anodic biofilm.

In contrast, when switching to the cathodic medium with fumarate and an applied potential of −0.44 V vs SHE, currents rapidly decayed to ca. −0.15 mA cm^{-2} and thereafter remained constant (Figure 3a). No lag phase or exponential growth was noted. Switching back to anodic mode once again gave rise to a new cycle of lag phase, exponential growth, and current plateau. However, each anodic growth required more time to reach the current plateau. Despite this, the plateau was observed in each case at a similar current density as the first anodic growth. Assuming the biofilm is already existing at a mature level because it reached a current plateau in the previous anodic growth, the current−time kinetic trace in this case is suggested to stem from an additional process besides biofilm growth. Each cathodic step, on the other hand,

https://dx.doi.org/10.1021/jacs.9b13077
J. Am. Chem. Soc. 2020, 142, 5194−5203

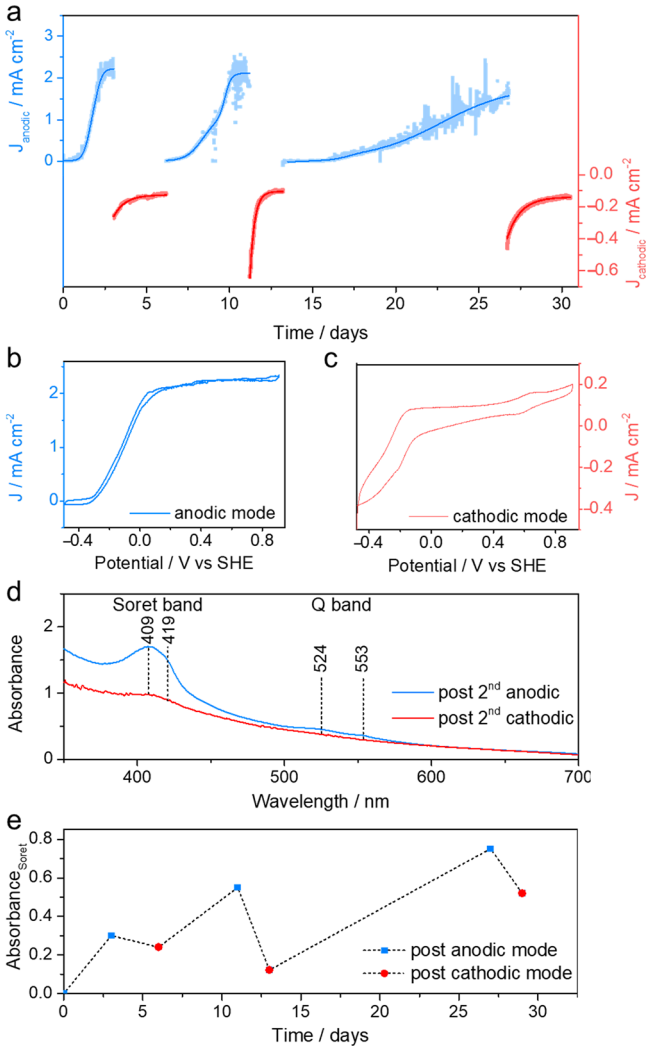

Figure 3. (a) Current−time traces of anodic and cathodic modes for *G. sulfurreducens* on the IO−ITO electrode. CVs recorded subsequently after (b) the first anodic and (c) the first cathodic mode steps under turnover conditions, i.e., in acetate and fumarate buffer media, respectively. (d) UV−vis spectra of *G. sulfurreducens* exhibit characteristic cytochrome bands in the Soret and Q-band region, which (e) vary in intensity, depending on the reaction mode (the maximum absorbance at 409 nm is plotted). The overall trend for the appearance and disappearance of the cytochromes is reversible for at least three cycles (UV−vis spectra from each cycle are shown in Figure S1).

exhibited similar current−time profiles with the exception of the very initial decay (Figure 3a). Cyclic voltammograms (CVs) after the first anodic and cathodic mode growth taken under turnover conditions (i.e., in the presence of substrate) showed a typical sigmoidal shape with a half-wave potential centered at −0.14 V vs SHE for anodic (Figure 3b) and approximately −0.2 V for cathodic (Figure 3c) modes.

UV−vis absorption spectra of the biofilm grown in anodic mode on IO−ITO electrodes featured strong bands at 409 and 419 nm for the oxidized and reduced species, respectively, arising from the well-known Soret absorption of the heme units of the *G. sulfurreducens* cytochromes (Figure 3d). After switching to cathodic mode, the intensity of the Soret band with the maximum at λ = 409 nm (representing the oxidized cytochrome species) is significantly decreased. Returning back to anodic mode resulted in an increase once more of the Soret band intensities, and again, these decreased after switching to cathodic mode (Figure 3e). As the measured absorbance is proportional to the concentration of heme units, the measurements suggest that the total amount of cytochromes increases after every anodic mode cycle, whereas after each cathodic mode step the overall cytochrome amount seems to be decreasing. We believe the first lag phase to stem from a combination of bacteria attaching to the electrode, extracellular matrix formation, and cytochrome expression necessary for EET. Initially the cells are grown in a fumarate-containing medium. The change from a soluble electron acceptor (fumarate) to an insoluble electron acceptor (electrode) may lead to a lengthy adaptation time for the cells to perform electrode respiration. Cytochromes are partially depleted during the cathodic mode, which suggests that their build-up is linked to longer anodic mode lag phases in the 2nd and 3rd cycles.

QCM-D is emerging as a powerful tool to probe the interaction of biological materials with inorganic substrates.[33,35−38] As a sample flows over and attaches to a piezoelectric quartz chip, the chip's resonance frequency and dissipation (rate of frequency decay) shift is proportional to the materials' mass. We used this technique to obtain a complementary set of mechanistic insights into *G. sulfurreducens*' growth behavior (Figure 4a). Biofilm growth was carried out directly in a QCM-D cell (Figure S2), which allowed us to monitor the biofilm's current−time profile and correlate to its mass increase (Figure 4b and 4c). A planar quartz chip coated with a planar thin ITO film (commercially purchased) was used to resemble the standard growth conditions employed earlier on the IO−ITO electrode.

To induce biofilm growth, the anodic growth medium was flown through the QCM-D cell and an aliquot of *G. sulfurreducens* injected once the time-dissipation trace exhibited stable behavior at ∼0.3 V vs SHE for >12 h. The change in dissipation was used as a qualitative proxy for mass change rather than the change in frequency due to the thick, viscoelastic nature of the biofilm.[35,36] Because of the inherent characteristics of the film (thickness and composition), the QCM-D measurements here qualitatively illustrate trends rather than quantify precise mass changes.

We observed an immediate start of increase in dissipation following injection of the cells, whereas the current remained minimal for at least 12 h (Figure 4b). A part of this increase at the beginning can be rationalized by sedimentation and attachment of the cells to the electrode surface. However, the continual rise of dissipation for more than 12 h (circulation was stopped after 15 min) suggests that the initial stages of *G. sulfurreducens* biofilm growth proceed even without significant electron transfer to/from the electrode. This is contrary to the speculation that the lag phase consists of minimal biofilm growth and that biofilm growth is only initiated in the exponential growth phase. In agreement, previous QCM-D studies have found the first stages of initial bacterial attachment (sedimentation) plateaus within 1−2 h.[39−42]

The dissipation slowed down after this initial increase and then began to rise again at ∼2−3 days. This time the current also began to rise exponentially after undergoing the previously mentioned lag phase (Figure 4c). Because this rise in current occurred after an initial biofilm was established, we speculate that the rise in current may be correlated to an enhanced expression of cytochromes within each bacterium cell for EET

https://dx.doi.org/10.1021/jacs.9b13077
J. Am. Chem. Soc. 2020, 142, 5194−5203

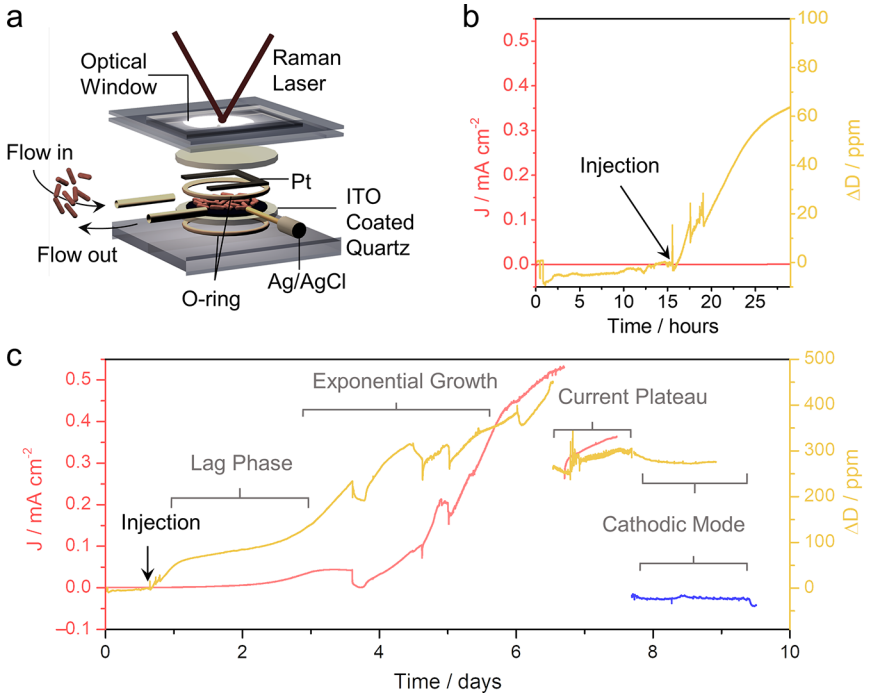

Figure 4. (a) Customized QCM-D cells were used to grow biofilms and acquire resonance Raman spectra. (b) The mass of biofilm growth (yellow trace) begins to increase immediately after *G. sulfurreducens* injection while the current (red trace) remains in lag phase. (c) After 2 days, both the anodic mode current (red trace) and the mass of biofilm growth (yellow trace) increase, and the mass remains constant when switching from anodic to cathodic mode. The cathodic mode current is illustrated in blue.

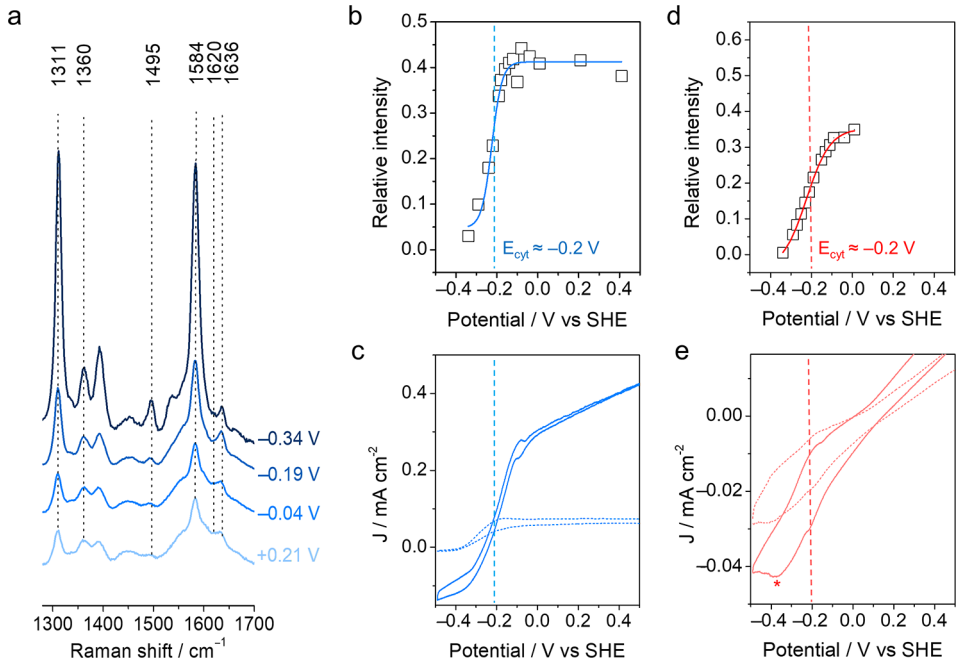

Figure 5. (a) 532 nm resonance Raman spectra of *G. sulfurreducens* grown under anodic conditions exhibit changes to the cytochrome spectra as the potential is varied under nonturnover conditions. Fitting the spectra reveals a redox transition from Fe(II) to Fe(III) that matches the midpoint of the catalytic rise in the CV under turnover conditions for both biofilms grown in (b, c) anodic and (d, e) cathodic conditions. The asterisk denotes a redox peak that does not correspond to a detectable spectral change of the cytochrome marker bands in the resonance Raman spectrum. CVs under turnover conditions are illustrated as solid and nonturnover as dashed lines.

rather than only biofilm growth. Both the current and the dissipation kept rising, though with different profiles, until ~7 days. A small decrease at 7 days stems from a piece of biofilm visibly detaching from the ITO electrode due to the medium circulation. Drops within the current–time trace between 4 and 6 days stem from restarting circulation, but overall the current–time profile is comparable to that of the growth on IO–ITO electrodes.

After 7.5 days, a bacteria-free cathodic medium was circulated through the QCM-D cell and the electrode was

https://dx.doi.org/10.1021/jacs.9b13077
J. Am. Chem. Soc. 2020, 142, 5194–5203

switched to −0.44 V vs SHE. The current in cathodic mode was constant at −0.02 mA cm^{-2} and the mass remained unchanged. This provides a further level of insight into the anodic−cathodic switching behavior of the *G. sulfurreducens* biofilm: the cytochromes appear suppressed, while the biofilm mass largely remains when switching to cathodic mode.

In situ resonance Raman (RR) spectroelectrochemistry was subsequently utilized to provide molecular level insights into the cytochrome characteristics. A 532 nm laser was used, which matches the Q-band absorption of the cytochromes in their reduced state (Figure 3d), significantly enhancing the resultant Raman signal. RR spectroelectrochemical experiments were carried out under nonturnover conditions, i.e., in fresh buffer medium that did not contain any substrate (acetate or fumarate). Shown are data from the biofilm grown on the planar QCM chip because of the higher signal intensities of the cell configuration. For reference, spectra of the biofilm grown on IO−ITO are shown in Figures S3 and S4. The RR spectra of *G. sulfurreducens* grown on ITO feature indicative bands at 1311 (ν_{21}), 1360 ($\nu_{4,red}$), 1495 ($\nu_{3,red}$), 1584 ($\nu_2/\nu_{19,ox}$), 1620 ($\nu_{10,red}$), and 1636 cm^{-1} ($\nu_{10,ox}$) (Figure 5a). The band frequencies are comparable to those observed in reported RR spectra for *G. sulfurreducens* and can be assigned to *c*-type cytochromes that dominate the RR spectra at this excitation wavelength.[43]

Upon increasing the potential stepwise from −0.34 to 0.21 V (vs SHE), the relative intensities of the bands changed, although the band positions did not shift. Significant band shifts as usually observed for isolated cytochromes upon changing the heme redox state (i.e., ferrous to ferric) were not observed. Such a behavior has already been noted and attributed to the fact that RR monitors a variety of cytochromes in the biofilm in different (mixed) oxidation/ligation states, which are present throughout the biofilm and react differently to the applied electrode potential.[44] In this respect, applying potentials affects only a part of the RR spectroscopically monitored cytochromes. This can be best visualized by the 1636 cm^{-1} band, which likely originates from the ν_{10} mode of the oxidized heme in a six-coordinated low-spin state with a His-Fe−X axial ligation (X being a strong ligand), which is visible at −0.34 V (vs SHE), i.e., reducing conditions. Outer-membrane cytochromes have been reported to give rise to a strong mode at 1639−40 cm^{-1} resulting from a His/His axial heme ligation pattern, whereas cytochrome *c* with His/Met as axial ligands can be monitored around 1636 cm^{-1}. Upon stepwise oxidation, the band at 1636 cm^{-1} was accordingly found to increase in relative intensity, while bands at 1360 and 1495 cm^{-1} originating from the ferrous hemes diminished. This indicates an increase in the relative concentration of oxidized hemes with increasing the electrode potential.

To estimate the apparent redox potential, component fit analysis was performed.[45] In contrast to an excitation at the Soret band, using 532 nm yields less intense RR spectra of the heme units along with a significant selective enhancement of the ferrous over the ferric state. This complicates the spectral analysis to quantify the potential-dependent distribution of redox states. To extract quantitative information, an alternative approach was therefore employed. As it was not possible to obtain a "pure" redox state of a thick biofilm, i.e., fully oxidized and reduced hemes, the spectra at −0.34 and 0.21 V were fitted and treated as two separate spectral compounds (Table S1). In this way, the different redox equilibria present between −0.34 and 0.21 V (vs SHE) have been monitored and the recorded spectra fitted for the intermediate potentials. Examples of fitted spectra are shown in Figure S5a, and the resulting relative concentration as a function of potential is plotted in Figure S5b. Note that the intrinsic relative cross-section difference for ferric and ferrous hemes in the different ligation states was not considered in this approach. Nevertheless, the analysis procedure yielded an apparent redox potential at approximately −0.2 V vs SHE, matching the redox transition at the midpoint of the catalytic trace in the biofilm CVs under turnover conditions (Figure 5b and 5c). This observation supports the change in the redox state of the cytochromes being related to the overall current flow via EET throughout the biofilm.[46,47]

A similar behavior and no major spectral differences were noted for biofilms treated under cathodic conditions (Figures 5d, 5e, and S6). This indicates that under both anodic and cathodic conditions the redox state distribution (though not the overall quantity) of cytochromes is comparable. An additional band at 1624 cm^{-1} that seems to be more pronounced at oxidizing conditions could be observed, which has been also reported when ITO is employed as an electrode.[43,44] However, the 1624 cm^{-1} band may also arise from a ν_{10} mode of the remaining reduced hemes at this potential that becomes more visible as other bands in the vicinity decline in relative intensity. Component fit analysis yields a redox potential at around −0.2 V (vs SHE) (Figure 5d), matching the catalytic trace under cathodic conditions (Figure 5e) as well as the transition found for biofilms grown under anodic potentials (Figure 5b). In both anodic and cathodic modes, the RR-derived redox potential matches the redox potential of the cytochrome determined from cyclic voltammetry experiments under nonturnover conditions (Figure 5c and 5e). We observe a second peak in the cathodic mode CV under nonturnover conditions that is centered around −0.34 V vs SHE, which may represent another species involved in the EET process in cathodic mode. As we do not detect any other cytochromes in the RR spectra (Figures S7 and S8), this redox couple does likely not arise from a cytochrome. Furthermore, CVs of biofilms after anodic mode do not exhibit this peak. However, due to the low(er) RR sensitivity at 532 nm, the involvement of a cytochrome cannot be fully ruled out.

In the presence of acetate, no major spectral differences could be spotted in the RR spectra (Figure S9). However, component fit analysis performed on RR spectra in the potential range from −0.44 to 0.21 V (vs SHE) showed that the potential-dependent spectral changes are less pronounced than in the absence of substrate (Figure S10; 16−40%). This corresponds to a smaller fraction of hemes within the biofilm changing their respective redox states following the poised electrode potential. This is in line with previous reports which detected a majority of reduced hemes also at oxidative potentials as they are functioning as electron relays in the catalytic process.[47]

The RR experiments bring forth several key points. (i) The half-wave of the catalytic currents is centered with the midpoint of the cytochrome redox potential. This implies that the cytochromes are facilitating EET in both anodic and cathodic directions. However, because of the greatly diminished signals of the cytochromes following the cathodic mode steps, they are likely not as abundant in that situation. (ii) We do not detect any other type of cytochrome after the

https://dx.doi.org/10.1021/jacs.9b13077
J. Am. Chem. Soc. 2020, 142, 5194−5203

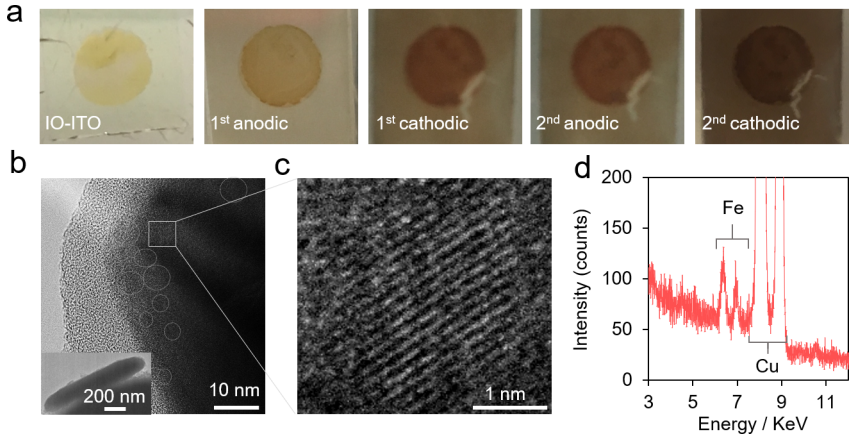

Figure 6. (a) Biofilm-grown IO−ITO electrode turns consecutively dark red following each cathodic step. (b, c) TEM images of *G. sulfurreducens* cells following cathodic mode show small, crystalline nanoparticles decorating the bacterium cell wall. (d) EDS point analysis of the cell's surface exhibits peaks stemming from Fe species; Cu peaks stem from TEM grid.

cathodic mode under our experimental conditions. This means that *G. sulfurreducens* does not express a significant amount of different cytochromes to facilitate its EET in cathodic mode. Furthermore, the second peak at −0.34 V in the CV after the cathodic mode likely does not correspond to a cytochrome as no spectral changes in the RR data were observed at this potential.

After each cathodic step we noted a color change of the IO−ITO electrode, which became progressively darker red (Figure 6a). We also observed that the bacteria-free electrolyte solution turned dark brown-red after each cathodic step. Postanodic conditions did not change the electrode's color, and the bacteria-free solution turned light red as planktonic bacteria appeared in the solution over time. The UV−vis spectrum of the red-brown solution postcathodic step displayed almost no bands related to cytochromes but an additional absorption peak at ∼620 nm, which could stem from FeO_x species in solution and/or on bacteria in solution (Figure S11). This iron species seems to be forming both in solution and throughout the biofilm under cathodic mode as the concentration of the Fe-containing cytochromes decreased. To investigate the possible formation of FeO_x particles, we transferred some *G. sulfurreducens* from the biofilm electrode after the second cathodic step to a TEM grid and imaged the bacteria at high magnifications. We discovered that the surface region of the cells was decorated with a series of ∼2−4 nm crystalline particles (Figure 6b and 6c). Lattice fringes of 2.51 and 2.15 Å were measured, which may correspond to the theoretical *d*-spacings for the Fe_2O_3 (002) and (112) planes, respectively. Energy-dispersive X-ray spectroscopy (EDS) point analyses of this region exhibited peaks attributed to Fe and Cu (the latter from the Cu TEM grid; Figure 6d). The *G. sulfurreducens* prior to growth on the electrode did not exhibit any crystalline particles on the cells' outer membrane (Figure S12). With this observation, we believe that the color change of the electrode following the cathodic step stems from the formation of FeO_x particles by *G. sulfurreducens*. However, we cannot unambiguously distinguish whether the FeO_x particles were formed directly on the bacteria membrane or precipitated from solution following their formation.

Biomineralization is present in a wide array of microorganisms and is now observed to be at play in these specific cathodic step conditions.[48] *G. sulfurreducens* have been shown to precipitate nanoparticles of Pd,[49] Au,[50] and Ag.[51] A wide array of Fe oxides can also form through biomineralization.[52] In the cathodic mode, lower amounts of cytochromes are used in comparison to the amount in anodic mode. As such, in the cathodic mode excess Fe(III) from the cytochromes may be reduced to Fe(II) as part of the bacterial metabolic process. This solubilized Fe(II) could, in a subsequent step, be oxidized back to solid Fe(III) on the cell membrane. The source of Fe for the FeO_x particles we found could be the cytochromes, which may not be needed to the same extent and partially degrade under cathodic mode conditions or from the Fe-containing cathodic buffer medium. Given these observations, the cytochromes seem not to be as heavily involved in the EET process under cathodic conditions and we hypothesize that Fe may be involved in the cathodic EET process, possibly as a redox mediator.

To ascertain the potential source of the Fe that gives rise to surface FeO_x particles, we first grew the *G. sulfurreducens* biofilm on an IO−ITO electrode under standard conditions (note, Fe was necessary in the initial anodic medium to achieve biofilm growth) and then switched to cathodic mode but using an Fe-free cathodic buffer medium (Figure 7). We noted that instead of a slowly decreasing current, the cathodic current−time trace showed a rapid decay and then an increase in the current magnitude. One possible explanation of this is that Fe species are involved in the cathodic EET process but need to

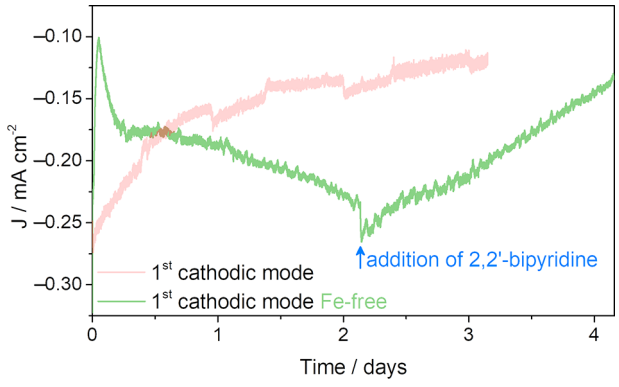

Figure 7. Current−time trace of *G. sulfurreducens* biofilm on IO−ITO with (red) and without (green) Fe ions in the buffer medium under cathodic conditions. The blue arrow indicates addition of 2,2′-bipyridine to the electrolyte solution.

https://dx.doi.org/10.1021/jacs.9b13077
J. Am. Chem. Soc. 2020, 142, 5194−5203

be first extracted from the cytochromes acting as an Fe source. Adding 10 mM of 2,2′-bipyridine to the cathodic step solution resulted in a decrease in the current density as Fe species were perhaps steadily complexed by 2,2′-bipyridine and no longer available for the EET pathway of *G. sulfurreducens* (Figure 7).[53] Discrepancies in the current densities between the individual biofilms after 2 days likely stem from the natural biofilm variance.

DISCUSSION AND CONCLUDING REMARKS

Putting together the entirety of our data, we formulate a plausible mechanism behind our results. The first stage of biofilm growth consists of the cells attaching to the electrode and biofilm growth. Following initial growth (which is evidenced to occur immediately through QCM-D measurements), the exponential current increase in anodic mode is thought to be enabled by the expression of cytochromes, as previously established.[1,16,20] Upon switching to cathodic mode, the biofilm mass remains intact but the same quantity of cytochromes is not necessary; thus, some of them may degrade to release Fe species. These soluble Fe species could act as redox mediators and/or are eventually released from the cells as a byproduct and "stored" in the form of FeO_x nanoparticles on the cell membrane (Figure 8). Therefore, the Fe species are speculated to be involved in the cathodic EET process.

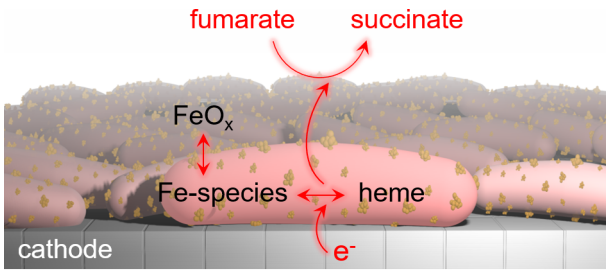

Figure 8. Possible EET pathway under cathodic reaction conditions.

This observation falls in line with previous gene-deletion studies on *G. sulfurreducens* that suggested that cytochromes were not as involved in cathodic mode EET as they were in anodic mode.[25] In situ infrared spectroelectrochemical studies of *Geobacter soli* biofilms also concluded that cathodic nitrate reduction proceeds through a different electron conduit than anodic acetate oxidation.[54] Furthermore, solubilized Fe species have been implicated in EET in *Shewanella oneidensis* MR-1 biofilms.[55]

In all, we probed mechanisms of EET between *G. sulfurreducens* and ITO electrodes using a host of techniques that were utilized on this system, such as in situ QCM-D and RR spectroelectrochemistry. While cytochrome expression is vital for anodic growth, we have found evidence that under cathodic conditions, the cytochromes partially degrade and their Fe is possibly utilized as a soluble redox species mediated in the EET process and the excess Fe precipitates in the form of FeO_x nanoparticles on the *G. sulfurreducens* surface. As we believe that cytochromes may be the Fe source for FeO_x particle formation, we can speculate that FeO_x particle formation/depletion is reversible to some extent. It remains to be seen whether or not the FeO_x particles participate in EET or are simply a byproduct and if *G. sulfurreducens* can function entirely without outer-membrane cytochromes in cathodic mode. Previous studies with *Shewanella* have found FeS particles that form on the cells' surface and that Fe_2O_3 and FeOOH particles added to the growing biofilm can even function as a bridge that facilitates EET.[56,57] While switching back to anodic conditions with bacteria-free solutions is possible and similar current plateaus can be attained, the change in biofilm composition is reflected in the longer amount of time it takes to do so after every cathodic step. In all, advancing the forefront of cell-based bioelectrochemical systems through the implementation of new techniques and routes of analysis is important to both extract fundamental insights into natural systems and develop functional biotechnological platforms.

EXPERIMENTAL DETAILS

Preparation of IO−ITO Electrodes. IO−ITO electrodes (10 μm) were prepared as previously reported.[28,30,31] Briefly, polystyrene microspheres served as a hard template for 10 μm pores. An array of them was filled with commercially purchased ITO nanoparticles (Sigma-Aldrich). Following the infiltration, the electrode was calcined in air (500 °C) at a 1 °C min^{-1} ramp rate to remove the polystyrene and sinter the ITO. The ITO was then cleaned by UV−Ozone treatment and ready to use. Typically, IO−ITO electrodes with a 0.25 cm^{-2} geometric surface area were used.

Bacteria Culturing. *G. sulfurreducens* PCA (DSM No. 12127) was purchased from the Leibniz-Institute DSMZ-German Collection of Microorganisms and Cell Cultures. *G. sulfurreducens* was cultured in anaerobic vials with 20 mM acetate as the electron donor and 50 mM fumarate as the electron acceptor in defined media.[14] The vials were purged with N_2:CO_2 (80:20 v:v %) for 1 h to keep the medium anaerobic. The inoculated vials were kept in a shaking incubator (30 °C, 180 rpm) for 5 days to grow anaerobically. The bacterial growth was monitored by measuring the optical density ($OD_{600\ nm}$) using a UV−vis spectrometer. Prior to inoculating the bioelectrochemical reactor, the as-grown bacterial solutions were centrifuged (7000 rpm, 4 min) and washed with fresh media twice to remove all possible media contaminations.

Biofilm Growth. A three-electrode system was used for conducting all of the bioelectrochemical experiments. As-prepared IO−ITO (surface area = 0.25 cm^2) was employed as the working electrode. Ag/AgCl (in 3 M NaCl solution) and a graphite rod were used as reference and counter electrodes, respectively. All potentials collected with the Ag/AgCl (3.0 M KCl) reference electrode are converted to reference SHE ($E_{SHE} = E_{Ag/AgCl} + 0.21$ V). The medium solution (19 mL) with 40 mM acetate (electron donor) was added into the reactor, and the solution was purged with N_2:CO_2 (80:20 v:v %) for 45 min. The as-grown *G. sulfurreducens* (1 mL) was inoculated into the medium solution (final OD = 0.6 in total 20 mL). The working IO−ITO electrode was poised at a potential of ∼0.3 V vs SHE, and the reactor was kept stirring (200 rpm) at a constant temperature (30 °C). After getting a stable anodic current, the reactor was switched to cathodic mode by replacing the medium with a fresh medium containing 20 mM fumarate as the electron acceptor and applying a potential of −0.44 V vs SHE by keeping anaerobic condition (purged with N_2:CO_2 for 45 min).

UV−vis Spectroscopy. UV−vis spectra were acquired with a Varian Cary 50 Bio UV−vis spectrometer. The reaction cell was placed in its entirety in the optical path of the light, and spectra were acquired without the need to remove the electrode from its air-free reaction environment. Typically, spectra were acquired after each growth mode.

QCM-D. QCM-D experiments were performed using a Biolin Q-sense explorer module and a customized QCM-D cell that featured electrodes (Ag/AgCl reference and Pt counter) for simultaneous electrochemical measurements, and a transparent window overtop that enabled RR spectroscopy to be carried out.[58] An AT-cut quartz chip functioned as the QCM-D substrate and working electrode. The quartz chip (purchased from Biolin scientific) was coated with a planar ITO film and was cleaned with sonication in Hellmanex

https://dx.doi.org/10.1021/jacs.9b13077
J. Am. Chem. Soc. 2020, 142, 5194−5203

surfactant (1% wt. in water) and in water for 15 min each prior to use. The third harmonic was used for analysis. Prior to biofilm growth, an air-free anodic growth medium was recirculated through the QCM-D setup and the signal was allowed to equilibrate for at least 12 h to ensure that signal drift was not a significant contributor to the data. Afterward, the bacteria were injected and circulation stopped after ~15 min to facilitate cell attachment and biofilm growth. Once the current began to decay due to the depletion of nutrients, the system was switched back to recirculation mode (0.141 mL min^{-1}). Switching to cathodic mode simply entailed switching to cathodic media under recirculation conditions and changing the electrochemical bias from 0.3 to −0.44 V vs SHE.

Resonance Raman Spectroscopy. RR spectra were acquired with a Horiba Labram Evolution spectrometer and 532 nm diode laser (~20 mW power). The standard reaction cell or the customized QCM-D cell were placed in the path of a long working distance 50× objective while still being wired to the potentiostat. Spectra were acquired at full power illumination, and typical acquisition times of 180 s were utilized. The focal point of the Raman objective was chosen for all electrodes in the same manner with a focus set directly onto the interface with the electrode surface and the biofilm. We probed mainly the bottom micrometer of the biofilm. The reversibility of the spectra suggests that the laser did not permanently damage the biofilm.

Scanning Electron Microscopy. To prepare electrodes for SEM, the biofilm was first stained with an osmium-based compound. Following this, the electrodes were dried by successively switching to ethanol−water mixtures with progressively higher ethanol contents. The electrodes were not coated with any conductive layer prior to imaging, and cross-section images were acquired by breaking the electrode in half and imaging. A TESCAN MIRA3 FEG-SEM operating at 5 kV was used for all SEM measurements.

Transmission Electron Microscopy. Samples were prepared for TEM analysis by rubbing a 300 mesh copper TEM grid containing a continuous carbon film against the biofilm-coated IO−ITO electrode and allowing the grid to dry under ambient conditions. A Thermo Scientific (FEI) Talos F200X G2 TEM operating at 200 kV was utilized for TEM analysis. TEM images were acquired using a Ceta, 4k × 4k CMOS camera. A Super-X EDS detector system with four windowless silicon-drift detectors was utilized for EDS analysis.

■ ASSOCIATED CONTENT

Supporting Information

The Supporting Information is available free of charge at https://pubs.acs.org/doi/10.1021/jacs.9b13077.

Band positions employed for the component fitting routine; UV−vis spectra of *G. sulfurreducens* show characteristic cytochrome bands in the Soret and Q-band regions; cross-section SEM images at low and high magnification; 532 nm RR spectra of *G. sulfurreducens* grown on IO−ITO under anodic mode at different applied electrode potentials; 532 nm RR spectra of *G. sulfurreducens* on IO−ITO in cathodic mode at different applied electrode potentials; Raman component fitting of *G. sulfurreducens* biofilms grown under anodic mode conditions; Raman component fitting of *G. sulfurreducens* biofilms grown under cathodic mode conditions; 532 nm RR spectra of *G. sulfurreducens* grown on planar ITO in cathodic mode at different applied electrode potentials; 532 nm RR spectra of *G. sulfurreducens* on planar ITO after cathodic mode switch at different applied electrode potentials; 532 nm RR spectra of *G. sulfurreducens* grown on planar ITO in anodic mode at different applied electrode potentials; 532 nm RR spectra of *G. sulfurreducens* grown on planar ITO under anodic mode at different applied electrode potentials; UV−vis spectra of medium (electrolyte) solution after anodic and cathodic conditions applied to *G. sulfurreducens* biofilm grown onto IO−ITO electrodes; TEM images of the *G. sulfurreducens* at low and high magnification prior to the cathodic step (PDF)

■ AUTHOR INFORMATION

Corresponding Author

Erwin Reisner − *Department of Chemistry, University of Cambridge, Cambridge CB2 1EW, United Kingdom;* orcid.org/0000-0002-7781-1616; Email: reisner@ch.cam.ac.uk

Authors

Nina Heidary − *Department of Chemistry, University of Cambridge, Cambridge CB2 1EW, United Kingdom; Department of Chemistry, Université de Montréal, Montreal, Quebec H3C 3J7, Canada*

Nikolay Kornienko − *Department of Chemistry, University of Cambridge, Cambridge CB2 1EW, United Kingdom; Department of Chemistry, Université de Montréal, Montreal, Quebec H3C 3J7, Canada;* orcid.org/0000-0001-7193-2428

Shafeer Kalathil − *Department of Chemistry, University of Cambridge, Cambridge CB2 1EW, United Kingdom;* orcid.org/0000-0002-2001-2100

Xin Fang − *Department of Chemistry, University of Cambridge, Cambridge CB2 1EW, United Kingdom;* orcid.org/0000-0001-9275-0690

Khoa H. Ly − *Department of Chemistry, University of Cambridge, Cambridge CB2 1EW, United Kingdom; Fakultät für Chemie und Lebensmittelchemie, Technische Universität Dresden, Dresden 01062, Germany*

Heather F. Greer − *Department of Chemistry, University of Cambridge, Cambridge CB2 1EW, United Kingdom*

Complete contact information is available at: https://pubs.acs.org/10.1021/jacs.9b13077

Author Contributions

[§]N.H. and N.K.: These authors contributed equally.

Notes

The authors declare no competing financial interest.

■ ACKNOWLEDGMENTS

N.K. was supported by a Royal Society Newton International Fellowship, NF160054. E.R., X.F., and N.H. acknowledge the European Research Council (ERC) Consolidator Grant "MatEnSAP" (682833). S.K. was supported by a Marie Skłodowska-Curie Fellowship (EMES, 744317). K.H.L. acknowledges the Open Topic Postdoc Programme of the Technische Universität Dresden and the Marie Skłodowska-Curie Fellowship (VSHER, 701192). The TEM was funded through the EPSRC underpinning multiuser equipment call (EP/P030467/1).

■ REFERENCES

(1) Logan, B. E.; Rossi, R.; Ragab, A.; Saikaly, P. E. Electroactive microorganisms in bioelectrochemical systems. *Nat. Rev. Microbiol.* **2019**, *17*, 307−319.

(2) Light, S. H.; Su, L.; Rivera-Lugo, R.; Cornejo, J. A.; Louie, A.; Iavarone, A. T.; Ajo-Franklin, C. M.; Portnoy, D. A. A flavin-based extracellular electron transfer mechanism in diverse Gram-positive bacteria. *Nature* **2018**, *562*, 140−144.

(3) Shi, L.; Dong, H.; Reguera, G.; Beyenal, H.; Lu, A.; Liu, J.; Yu, H.-Q.; Fredrickson, J. K. Extracellular electron transfer mechanisms between microorganisms and minerals. *Nat. Rev. Microbiol.* **2016**, *14*, 651.
(4) Logan, B. E. Exoelectrogenic bacteria that power microbial fuel cells. *Nat. Rev. Microbiol.* **2009**, *7*, 375−381.
(5) Liu, C.; Colón, B. C.; Ziesack, M.; Silver, P. A.; Nocera, D. G. Water splitting−biosynthetic system with CO_2 reduction efficiencies exceeding photosynthesis. *Science* **2016**, *352*, 1210−1213.
(6) Nevin, K. P.; Woodard, T. L.; Franks, A. E.; Summers, Z. M.; Lovley, D. R. Microbial Electrosynthesis: Feeding Microbes Electricity To Convert Carbon Dioxide and Water to Multicarbon Extracellular Organic Compounds. *mBio* **2010**, *1*, No. e00103-10.
(7) Kornienko, N.; Zhang, J. Z.; Sakimoto, K. K.; Yang, P.; Reisner, E. Interfacing nature's catalytic machinery with synthetic materials for semi-artificial photosynthesis. *Nat. Nanotechnol.* **2018**, *13*, 890−899.
(8) Sakimoto, K. K.; Kornienko, N.; Yang, P. Cyborgian Material Design for Solar Fuel Production: The Emerging Photosynthetic Biohybrid Systems. *Acc. Chem. Res.* **2017**, *50*, 476−481.
(9) Lee, Y. V.; Tian, B. Learning from Solar Energy Conversion: Biointerfaces for Artificial Photosynthesis and Biological Modulation. *Nano Lett.* **2019**, *19*, 2189−2197.
(10) Potter, M. C. Electrical effects accompanying the decomposition of organic compounds. *Proc. R. Soc. London, Ser. B* **1911**, *84*, 260−276.
(11) Sakimoto, K. K.; Kornienko, N.; Cestellos-Blanco, S.; Lim, J.; Liu, C.; Yang, P. Physical Biology of the Materials−Microorganism Interface. *J. Am. Chem. Soc.* **2018**, *140*, 1978−1985.
(12) Caccavo, F.; Lonergan, D. J.; Lovley, D. R.; Davis, M.; Stolz, J. F.; McInerney, M. J. Geobacter sulfurreducens sp. nov., a hydrogen- and acetate-oxidizing dissimilatory metal-reducing microorganism. *Appl. Environ. Microbiol.* **1994**, *60*, 3752−3759.
(13) Nevin, K. P.; Richter, H.; Covalla, S. F.; Johnson, J. P.; Woodard, T. L.; Orloff, A. L.; Jia, H.; Zhang, M.; Lovley, D. R. Power output and columbic efficiencies from biofilms of Geobacter sulfurreducens comparable to mixed community microbial fuel cells. *Environ. Microbiol.* **2008**, *10*, 2505−2514.
(14) Bond, D. R.; Lovley, D. R. Electricity Production by Geobacter sulfurreducens Attached to Electrodes. *Appl. Environ. Microbiol.* **2003**, *69*, 1548−1555.
(15) Jiang, X.; Hu, J.; Petersen, E. R.; Fitzgerald, L. A.; Jackan, C. S.; Lieber, A. M.; Ringeisen, B. R.; Lieber, C. M.; Biffinger, J. C. Probing single- to multi-cell level charge transport in Geobacter sulfurreducens DL-1. *Nat. Commun.* **2013**, *4*, 2751.
(16) Nevin, K. P.; Kim, B.-C.; Glaven, R. H.; Johnson, J. P.; Woodard, T. L.; Methé, B. A.; DiDonato, R. J., Jr; Covalla, S. F.; Franks, A. E.; Liu, A. Anode biofilm transcriptomics reveals outer surface components essential for high density current production in Geobacter sulfurreducens fuel cells. *PLoS One* **2009**, *4*, No. e5628.
(17) Malvankar, N. S.; Tuominen, M. T.; Lovley, D. R. Lack of cytochrome involvement in long-range electron transport through conductive biofilms and nanowires of Geobacter sulfurreducens. *Energy Environ. Sci.* **2012**, *5*, 8651−8659.
(18) Snider, R. M.; Strycharz-Glaven, S. M.; Tsoi, S. D.; Erickson, J. S.; Tender, L. M. Long-range electron transport in Geobacter sulfurreducens biofilms is redox gradient-driven. *Proc. Natl. Acad. Sci. U. S. A.* **2012**, *109*, 15467−15472.
(19) Jain, A.; Gazzola, G.; Panzera, A.; Zanoni, M.; Marsili, E. Visible spectroelectrochemical characterization of Geobacter sulfurreducens biofilms on optically transparent indium tin oxide electrode. *Electrochim. Acta* **2011**, *56*, 10776−10785.
(20) Bond, D. R.; Strycharz-Glaven, S. M.; Tender, L. M.; Torres, C. I. On electron transport through Geobacter biofilms. *ChemSusChem* **2012**, *5*, 1099−1105.
(21) Thirumurthy, M. A; Jones, A. K *Geobacter* cytochrome OmcZs binds riboflavin: implications for extracellular electron transfer. *Nanotechnology* **2020**, *31*, 124001.
(22) Okamoto, A.; Saito, K.; Inoue, K.; Nealson, K. H.; Hashimoto, K.; Nakamura, R. Uptake of self-secreted flavins as bound cofactors for extracellular electron transfer in Geobacter species. *Energy Environ. Sci.* **2014**, *7*, 1357−1361.
(23) Gregory, K. B.; Bond, D. R.; Lovley, D. R. Graphite electrodes as electron donors for anaerobic respiration. *Environ. Microbiol.* **2004**, *6*, 596−604.
(24) Dumas, C.; Basseguy, R.; Bergel, A. Microbial electrocatalysis with Geobacter sulfurreducens biofilm on stainless steel cathodes. *Electrochim. Acta* **2008**, *53*, 2494−2500.
(25) Strycharz, S. M.; Glaven, R. H.; Coppi, M. V.; Gannon, S. M.; Perpetua, L. A.; Liu, A.; Nevin, K. P.; Lovley, D. R. Gene expression and deletion analysis of mechanisms for electron transfer from electrodes to Geobacter sulfurreducens. *Bioelectrochemistry* **2011**, *80*, 142−150.
(26) Rosenbaum, M.; Aulenta, F.; Villano, M.; Angenent, L. T. Cathodes as electron donors for microbial metabolism: Which extracellular electron transfer mechanisms are involved? *Bioresour. Technol.* **2011**, *102*, 324−333.
(27) Choi, O.; Sang, B.-I. Extracellular electron transfer from cathode to microbes: application for biofuel production. *Biotechnol. Biofuels* **2016**, *9*, 11.
(28) Fang, X.; Sokol, K. P.; Heidary, N.; Kandiel, T. A.; Zhang, J. Z.; Reisner, E. Structure−Activity Relationships of Hierarchical Three-Dimensional Electrodes with Photosystem II for Semiartificial Photosynthesis. *Nano Lett.* **2019**, *19*, 1844−1850.
(29) Mersch, D.; Lee, C.-Y.; Zhang, J. Z.; Brinkert, K.; Fontecilla-Camps, J. C.; Rutherford, A. W.; Reisner, E. Wiring of Photosystem II to Hydrogenase for Photoelectrochemical Water Splitting. *J. Am. Chem. Soc.* **2015**, *137*, 8541−8549.
(30) Fang, X.; Kalathil, S.; Divitini, G.; Wang, Q.; Reisner, E. A three-dimensional hybrid electrode with electroactive microbes for efficient electrogenesis and chemical synthesis. *Proc. Natl. Acad. Sci. U. S. A.* **2020**, 201913463.
(31) Zhang, J. Z.; Bombelli, P.; Sokol, K. P.; Fantuzzi, A.; Rutherford, A. W.; Howe, C. J.; Reisner, E. Photoelectrochemistry of Photosystem II in Vitro vs in Vivo. *J. Am. Chem. Soc.* **2018**, *140*, 6−9.
(32) Kalathil, S.; Katuri, K. P.; Alazmi, A. S.; Pedireddy, S.; Kornienko, N.; Costa, P. M. F. J.; Saikaly, P. E. Bioinspired Synthesis of Reduced Graphene Oxide-Wrapped Geobacter sulfurreducens as a Hybrid Electrocatalyst for Efficient Oxygen Evolution Reaction. *Chem. Mater.* **2019**, *31*, 3686−3693.
(33) Kornienko, N.; Ly, K. H.; Robinson, W. E.; Heidary, N.; Zhang, J. Z.; Reisner, E. Advancing Techniques for Investigating the Enzyme−Electrode Interface. *Acc. Chem. Res.* **2019**, *52*, 1439−1448.
(34) Robador, A.; LaRowe, D. E.; Finkel, S. E.; Amend, J. P.; Nealson, K. H. Changes in Microbial Energy Metabolism Measured by Nanocalorimetry during Growth Phase Transitions. *Front. Microbiol.* **2018**, *9*, 109.
(35) Olsson, A. L. J.; van der Mei, H. C.; Busscher, H. J.; Sharma, P. K. Acoustic sensing of the bacterium−substratum interface using QCM-D and the influence of extracellular polymeric substances. *J. Colloid Interface Sci.* **2011**, *357*, 135−138.
(36) Alexander, T. E.; Lozeau, L. D.; Camesano, T. A. QCM-D characterization of time-dependence of bacterial adhesion. *Cell Surf.* **2019**, *5*, 100024.
(37) Singh, K.; Blanford, C. F. Electrochemical Quartz Crystal Microbalance with Dissipation Monitoring: A Technique to Optimize Enzyme Use in Bioelectrocatalysis. *ChemCatChem* **2014**, *6*, 921−929.
(38) Miller, M.; Robinson, W. E.; Oliveira, A. R.; Heidary, N.; Kornienko, N.; Warnan, J.; Pereira, I. A. C.; Reisner, E. Interfacing Formate Dehydrogenase with Metal Oxides for the Reversible Electrocatalysis and Solar-Driven Reduction of Carbon Dioxide. *Angew. Chem., Int. Ed.* **2019**, *58*, 4601−4605.
(39) Olsson, A. L. J.; van der Mei, H. C.; Busscher, H. J.; Sharma, P. K. Influence of Cell Surface Appendages on the Bacterium-Substratum Interface Measured Real-Time Using QCM-D. *Langmuir* **2009**, *25*, 1627−1632.
(40) Olsson, A. L. J.; Wargenau, A.; Tufenkji, N. Optimizing Bacteriophage Surface Densities for Bacterial Capture and Sensing in

https://dx.doi.org/10.1021/jacs.9b13077
J. Am. Chem. Soc. 2020, 142, 5194−5203

Quartz Crystal Microbalance with Dissipation Monitoring. *ACS Appl. Mater. Interfaces* **2016**, *8*, 13698−13706.
(41) Gutman, J.; Walker, S. L.; Freger, V.; Herzberg, M. Bacterial Attachment and Viscoelasticity: Physicochemical and Motility Effects Analyzed Using Quartz Crystal Microbalance with Dissipation (QCM-D). *Environ. Sci. Technol.* **2013**, *47*, 398−404.
(42) Wang, Y.; Narain, R.; Liu, Y. Study of Bacterial Adhesion on Different Glycopolymer Surfaces by Quartz Crystal Microbalance with Dissipation. *Langmuir* **2014**, *30*, 7377−7387.
(43) Virdis, B.; Millo, D.; Donose, B. C.; Batstone, D. J. Real-Time Measurements of the Redox States of c-Type Cytochromes in Electroactive Biofilms: A Confocal Resonance Raman Microscopy Study. *PLoS One* **2014**, *9*, No. e89918.
(44) Robuschi, L.; Tomba, J. P.; Schrott, G. D.; Bonanni, P. S.; Desimone, P. M.; Busalmen, J. P. Spectroscopic Slicing to Reveal Internal Redox Gradients in Electricity-Producing Biofilms. *Angew. Chem., Int. Ed.* **2013**, *52*, 925−928.
(45) Millo, D.; Harnisch, F.; Patil, S. A.; Ly, H. K.; Schröder, U.; Hildebrandt, P. In Situ Spectroelectrochemical Investigation of Electrocatalytic Microbial Biofilms by Surface-Enhanced Resonance Raman Spectroscopy. *Angew. Chem., Int. Ed.* **2011**, *50*, 2625−2627.
(46) Fricke, K.; Harnisch, F.; Schröder, U. On the use of cyclic voltammetry for the study of anodic electron transfer in microbial fuel cells. *Energy Environ. Sci.* **2008**, *1*, 144−147.
(47) Ly, H. K.; Harnisch, F.; Hong, S.-F.; Schröder, U.; Hildebrandt, P.; Millo, D. Unraveling the Interfacial Electron Transfer Dynamics of Electroactive Microbial Biofilms Using Surface-Enhanced Raman Spectroscopy. *ChemSusChem* **2013**, *6*, 487−492.
(48) Crookes-Goodson, W. J.; Slocik, J. M.; Naik, R. R. Bio-directed synthesis and assembly of nanomaterials. *Chem. Soc. Rev.* **2008**, *37*, 2403−2412.
(49) Yates, M. D.; Cusick, R. D.; Logan, B. E. Extracellular Palladium Nanoparticle Production using Geobacter sulfurreducens. *ACS Sustainable Chem. Eng.* **2013**, *1*, 1165−1171.
(50) Tanzil, A. H.; Sultana, S. T.; Saunders, S. R.; Dohnalkova, A. C.; Shi, L.; Davenport, E.; Ha, P.; Beyenal, H. Production of gold nanoparticles by electrode-respiring Geobacter sulfurreducens biofilms. *Enzyme Microb. Technol.* **2016**, *95*, 69−75.
(51) Vasylevskyi, S. I.; Kracht, S.; Corcosa, P.; Fromm, K. M.; Giese, B.; Füeg, M. Formation of Silver Nanoparticles by Electron Transfer in Peptides and c-Cytochromes. *Angew. Chem., Int. Ed.* **2017**, *56*, 5926−5930.
(52) Miot, J.; Etique, M. *Formation and transformation of iron-bearing minerals by iron (II)-oxidizing and iron (III)-reducing bacteria*; Wiley-VCH Verlag GmbH & Co: Weinheim, Germany, 2016; pp 53−98.
(53) Estevez-Canales, M.; Kuzume, A.; Borjas, Z.; Füeg, M.; Lovley, D.; Wandlowski, T.; Esteve-Núñez, A. A severe reduction in the cytochrome C content of Geobacter sulfurreducens eliminates its capacity for extracellular electron transfer. *Environ. Microbiol. Rep.* **2015**, *7*, 219−226.
(54) Yang, G.; Huang, L.; You, L.; Zhuang, L.; Zhou, S. Electrochemical and spectroscopic insights into the mechanisms of bidirectional microbe-electrode electron transfer in Geobacter soli biofilms. *Electrochem. Commun.* **2017**, *77*, 93−97.
(55) Oram, J.; Jeuken, L. J. C. A Re-evaluation of Electron-Transfer Mechanisms in Microbial Electrochemistry: Shewanella Releases Iron that Mediates Extracellular Electron Transfer. *ChemElectroChem* **2016**, *3*, 829−835.
(56) Jiang, X.; Hu, J.; Lieber, A. M.; Jackan, C. S.; Biffinger, J. C.; Fitzgerald, L. A.; Ringeisen, B. R.; Lieber, C. M. Nanoparticle Facilitated Extracellular Electron Transfer in Microbial Fuel Cells. *Nano Lett.* **2014**, *14*, 6737−6742.
(57) Nakamura, R.; Kai, F.; Okamoto, A.; Hashimoto, K. Mechanisms of long-distance extracellular electron transfer of metal-reducing bacteria mediated by nanocolloidal semiconductive iron oxides. *J. Mater. Chem. A* **2013**, *1*, 5148−5157.
(58) Kornienko, N.; Heidary, N.; Cibin, G.; Reisner, E. Catalysis by design: development of a bifunctional water splitting catalyst through an operando measurement directed optimization cycle. *Chem. Sci.* **2018**, *9*, 5322−5333.

https://dx.doi.org/10.1021/jacs.9b13077
J. Am. Chem. Soc. 2020, 142, 5194−5203